

# Anisotropic Thermal Boundary Resistance across 2D Black Phosphorus: Experiment and Atomistic Modeling of Interfacial Energy Transport

Man Li, Joon Sang Kang, Huu Duy Nguyen, Huan Wu, Toshihiro Aoki, and Yongjie Hu\*

Interfacial thermal boundary resistance (TBR) plays a critical role in near-junction thermal management of modern electronics. In particular, TBR can dominate heat dissipation and has become increasingly important due to the continuous emergence of novel nanomaterials with promising electronic and thermal applications. A highly anisotropic TBR across a prototype 2D material, i.e., black phosphorus, is reported through a crystal-orientation-dependent interfacial transport study. The measurements show that the metal–semiconductor TBR of the cross-plane interfaces is 241% and 327% as high as that of the armchair and zigzag direction-oriented interfaces, respectively. Atomistic *ab initio* calculations are conducted to analyze the anisotropic and temperature-dependent TBR using density functional theory (DFT)-derived full phonon dispersion relation and molecular dynamics simulation. The measurement and modeling work reveals that such a highly anisotropic TBR can be attributed to the intrinsic band structure and phonon spectral transmission. Furthermore, it is shown that phonon hopping between different branches is important to modulate the interfacial transport process but with directional preferences. A critical fundamental understanding of interfacial thermal transport and TBR–structure relationships is provided, which may open up new opportunities in developing advanced thermal management technology through the rational control over nanostructures and interfaces.

thermal conductivity, such as cubic boron phosphide ( $\approx 500 \text{ W m}^{-1} \text{ K}^{-1}$ )<sup>[8]</sup> and boron arsenide ( $1300 \text{ W m}^{-1} \text{ K}^{-1}$ ).<sup>[7,13,14]</sup> In parallel to heat transfer in homogeneous materials, heat dissipation in high-power devices can also be severely limited by the near-junction thermal resistance across heterogeneous interfaces, i.e., the thermal boundary resistance (TBR).<sup>[1,2,4,12,15]</sup> On the other hand, thermal isolation applications, such as jet engine turbines, require interfaces with large TBR and high temperature stability.<sup>[16]</sup> Therefore, controlling TBR at the interfaces between different materials is of primary significance. However, the current understanding of TBR remains elusive and is far below that of heat transfer in homogeneous materials. Fundamentally, TBR measures an interface's resistance to thermal flow and results from the scattering of energy carriers, due to the difference in vibrational and electronic band structures from both sides of the interface. The earliest discovery of TBR can be traced back to 1941 and the Kapitza resistance between solids and liquid helium.<sup>[17]</sup> Thereafter, TBR was confirmed to exist at all heterogeneous

With the continuous miniaturization of modern electronic devices, power density increases dramatically in nanoscale chips and heat dissipation becomes a key technological challenge for the semiconductor industry.<sup>[1–12]</sup> Intensive efforts have been devoted to thermal management, including the recent development of new semiconductor materials with ultrahigh

interfaces regardless of the atomic perfection.<sup>[18]</sup> Despite decades of efforts, understanding and improving TBR still remains challenging. Most studies are usually limited to idealized interfaces or isotropic considerations, and a synergy between TBR and materials structures has not been well established.<sup>[19]</sup>

In the meantime, 2D van der Waals materials and their heterostructures are under intense exploration as building blocks for nanoelectronics, making studying heat dissipation across their interfaces of high interest.<sup>[20–25]</sup> Moreover, 2D materials are the ideal platform for exploring the structural relationship with TBR because of their highly orientation-dependent phonon band structures. In particular, black phosphorus (BP) has a highly anisotropic puckered orthorhombic crystal structure.<sup>[25–27]</sup> As illustrated in **Figure 1a**, each P atom forms three covalent bonds from the 3p orbitals. Inside each 2D lattice layer, there are two types of phosphorus bonds: the longer bond connects P atoms in the top and bottom planes, and the shorter bond connects the nearest P atoms in the same plane. The interlayer interaction is based on van der Waals forces.

M. Li, J. S. Kang, H. D. Nguyen, H. Wu, Prof. Y. Hu  
Department of Mechanical and Aerospace Engineering  
University of California  
Los Angeles, CA 90095, USA  
E-mail: yhu@seas.ucla.edu

T. Aoki  
Irvine Materials Research Institute  
University of California  
Irvine, CA 92697, USA

 The ORCID identification number(s) for the author(s) of this article can be found under <https://doi.org/10.1002/adma.201901021>.

DOI: 10.1002/adma.201901021

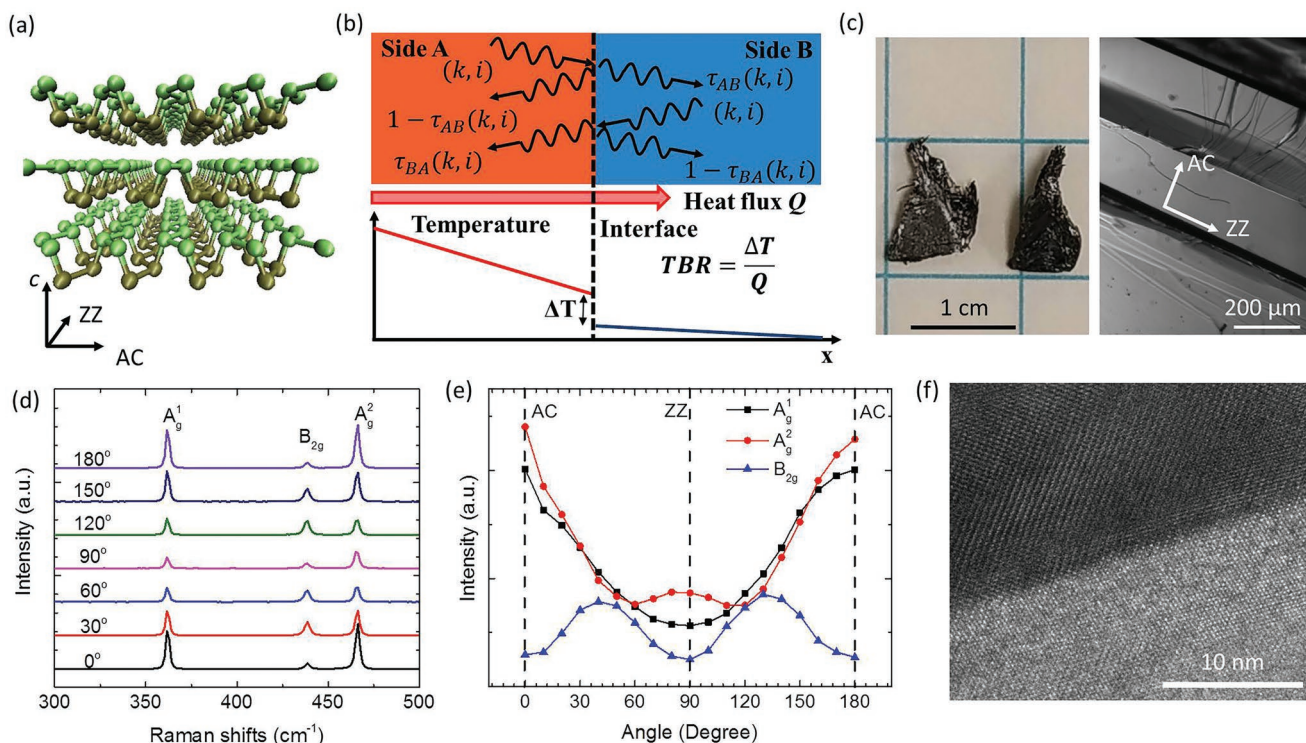


**Figure 1.** TBR and material characterization of BP. a) Schematic of the crystal structure of BP. b) Schematic of thermal transport and temperature profile across a material interface.  $\tau_{AB}$  represents the mode-specific transmission of phonons from material A to material B.  $k$  and  $i$  represent the phonon wave vector and polarization, respectively. An abrupt temperature drop ( $\Delta T$ ) at the material interface indicates a TBR that restricts the heat flux ( $Q$ ) going across the interface. c) Optical images of BP samples. d) Angle-dependent Raman spectroscopy of BP. e) The intensity plot of three Raman peaks with measurement angle dependence and used to determine the crystal orientations of BP. f) High-resolution transmission electron microscopy image of the interface between aluminum and black phosphorus.

So, there are three characteristic directions in BP defined as armchair (AC), zigzag (ZZ), and cross-plane (CP) directions (Figure 1a), which lead to their respective thermal conductivity of 85.80, 27.58, and 3.86 W m<sup>-1</sup> K<sup>-1</sup>.<sup>[28–34]</sup> In situ measurements conducted with ionic intercalations have also revealed anisotropic defect scattering on the phonon transport.<sup>[28]</sup> Therefore, BP can serve as a powerful platform to explore the mechanisms for the formation of TBR and its crystal structural relationship. As illustrated in Figure 1b, TBR is generally understood as resulting from the breakdown of coherence of energy carriers' transport across the interface. When the incident phonons encounter the interface, some of them transmit through the interface, while the remaining phonons are reflected by the interface. The sudden impedance to the phonon transport leads to discontinuous equilibrium distribution of phonons at the interface, i.e., a sharp temperature drop ( $\Delta T$ , Figure 1b). At steady state, the total heat flux ( $Q$ ) near the interface regime on both sides should match with each other. Therefore, as the heat flux is mainly carried by the phonons, the anisotropy of the phonon band structures of BP may result in different spectral phonon fluxes along different directions. However, on the metal side, the nearly isotropic structure will result in the same spectral heat flux regardless of the orientation. In the meanwhile, to conserve the energy flow across the interface, the spectral phonon transmissivity needs to be orientation dependent. Therefore, studying such interfacial energy transport across

directional 2D lattice could be strongly affected by the intrinsic anisotropic phonon spectra and provide direct TBR–structure relationships but remains unexplored so far.<sup>[19]</sup>

Here, we report the first investigation on the crystal-orientation-dependent thermal transport across metal–BP interfaces and observe highly anisotropic TBRs stemmed from the intrinsic structures. High-quality BP crystals were synthesized using the chemical vapor deposition method. Red phosphorus was used for starting material and SnI<sub>4</sub> and Sn as a mineralizer. 400 mg of red phosphorus with 20 mg of Sn and 10 mg of SnI<sub>4</sub> were grinded by using pestle and mortar. A quartz tube was preheated at 473 K under vacuum to remove possible moisture. After the red phosphorus, SnI<sub>4</sub>, and Sn mixture was loaded, the quartz tube was evacuated and flame-sealed under high vacuum. The tube was then placed into the two-zone tube furnace, with temperatures of 923 and 897 K for hot zone and cold zone, respectively. Furnace was slowly heated from room temperature to reaction temperature for 4 h and held for 24 h and slowly cooled down to room temperature. We are able to obtain centimeter-sized high-quality BP as shown in Figure 1c, indicating a clean surface after exfoliation. To prepare interfaces with different orientations, the crystalline directions of BP were identified first by angle-resolved, polarized Raman spectroscopy. When the incident laser beam was parallel to the cross-plane direction of BP, three Raman peaks were observed: A<sub>g</sub><sup>1</sup> ( $\approx 363$  cm<sup>-1</sup>),

$B_g^2$  ( $\approx 440 \text{ cm}^{-1}$ ), and  $A_g^2$  ( $\approx 467 \text{ cm}^{-1}$ )<sup>[28,35–37]</sup> (Figure 1d). The fact that the relative intensity of the three Raman peaks depends on the alignment of the angles between the polarization of the excitation laser and the crystal orientations is noteworthy. For example, the  $A_g^1$  and  $A_g^2$  peaks are maximized when the polarization is along the AC direction, whereas  $B_g^2$  peak achieves the highest intensity when the laser polarization forms a  $45^\circ$  angle with the AC direction. Therefore, the angle-dependent intensities of the three Raman peaks, plotted in Figure 1e, were used to determine the crystal orientations. The BP samples were cleaved along different orientations in parallel to the ZZ, AC, and CP directions, respectively. A thin layer of aluminum (Al) around 100 nm was deposited on the samples via e-beam evaporation to form a clean metal–semiconductor interface (Figure 1f).

TBR of metal–semiconductor interfaces along different crystal orientations of BP was characterized using a time-domain thermoreflectance (TDTR) technique, illustrated in Figure 2a. TDTR is an ultrafast technique that has been widely applied for measuring thermal properties and TBRs of different materials<sup>[7,8,38–42]</sup> and has been used to develop novel experimental spectroscopy techniques to study phonon spectra.<sup>[8,9,43]</sup> In our setup, a femtosecond laser pulse is split into a pump beam and a probe beam. The pump beam, at the wavelength of 400 nm, thermally excites the sample surface, and the probe beam, at the wavelength of 800 nm, detects the sample temperature. The delay time between pump and probe beams can be precisely controlled by a mechanical delay stage with a sub-picosecond resolution. The transient TDTR signal is detected and fitted to a multilayer thermal model to extract TBR. The typical experimental data from our TDTR measurements and fittings,<sup>[40]</sup> based on the phase signals for the ZZ, AC, and CP directions, are shown in Figure 2b. Surprisingly, a significantly high ratio of anisotropic TBRs for BP–Al interfaces was measured for different BP crystal orientations. TBR in the cross-plane direction ( $TBR_{CP}$ ) is  $1.62 \times 10^{-8} \text{ m}^2 \text{ K W}^{-1}$ , 2.41 times of that in the AC direction ( $6.71 \times 10^{-9} \text{ m}^2 \text{ K W}^{-1}$ ) and 3.27 times of that in the ZZ direction ( $4.95 \times 10^{-9} \text{ m}^2 \text{ K W}^{-1}$ ). To further investigate the phonon transport mechanism at the BP–Al interface, we also measured the temperature-dependent

TBR in each direction from 80 to 300 K. The anisotropy of TBR along different orientations remains remarkable for the full temperature range. Such a high ratio of anisotropic TBR has not been observed in other material interfaces.<sup>[19]</sup> We attribute the observed substantial TBR anisotropy to the highly anisotropic crystal structures, thus the anisotropic phonon band structures of BP, and combine theory and experiment to perform detailed analysis in the following.

To quantitatively analyze the crystal orientation and temperature-dependent anisotropic TBR, we performed ab initio calculations to capture phonon spectral contributions. From the phonon picture,<sup>[44]</sup> TBR can be understood as phonon reflection by interface. By integrating all the energy carried by the transmitted phonons, TBR or its reciprocal value, i.e., thermal boundary conductance ( $G$ ), can be calculated as

$$\frac{1}{TBR} = G = \frac{1}{2(2\pi)^3} \sum_i \int_{\mathbf{k}} \tau_{AB}(\mathbf{k}, i) \hbar \omega(\mathbf{k}, i) |\mathbf{v}(\mathbf{k}, i) \cdot \mathbf{n}| \frac{df}{dT} d\mathbf{k} \quad (1)$$

where  $\tau_{AB}(\mathbf{k}, i)$ ,  $\omega(\mathbf{k}, i)$ ,  $\mathbf{v}(\mathbf{k}, i)$ , and  $f = 1/\{\exp[\hbar\omega(\mathbf{k}, i)/k_B T] - 1\}$ , respectively, are the mode-dependent transmission coefficient, phonon frequency, group velocity, and equilibrium Bose–Einstein distribution function corresponding to phonons with wave vector  $\mathbf{k}$  and polarization  $i$ .  $\mathbf{n}$  is the unit vector normal to interface. The calculation of TBR requires a detailed knowledge of the phonon dispersion relationship over the entire Brillouin zone. In the literature, for simplicity, the dispersion relationship is usually approximated by a linear dispersion relationship (i.e., the Debye approximation<sup>[45]</sup>). However, the Debye approximation oversimplifies the TBR calculation using a single phonon group velocity along each direction. Reddy et al.<sup>[46]</sup> improved the Debye approximation by using the Born–von Karman model instead of the linear assumption in the Debye model. Dames and co-workers<sup>[47]</sup> proposed elliptical dispersion relations to account for the anisotropic phonon band structure.

Here, we performed ab initio calculations to obtain the full phonon dispersion relationship and construct the phonon-mode-dependent modeling of the interfacial thermal transport. To obtain the full phonon dispersion relationship of BP and Al, the second-order interatomic force constants are needed for the

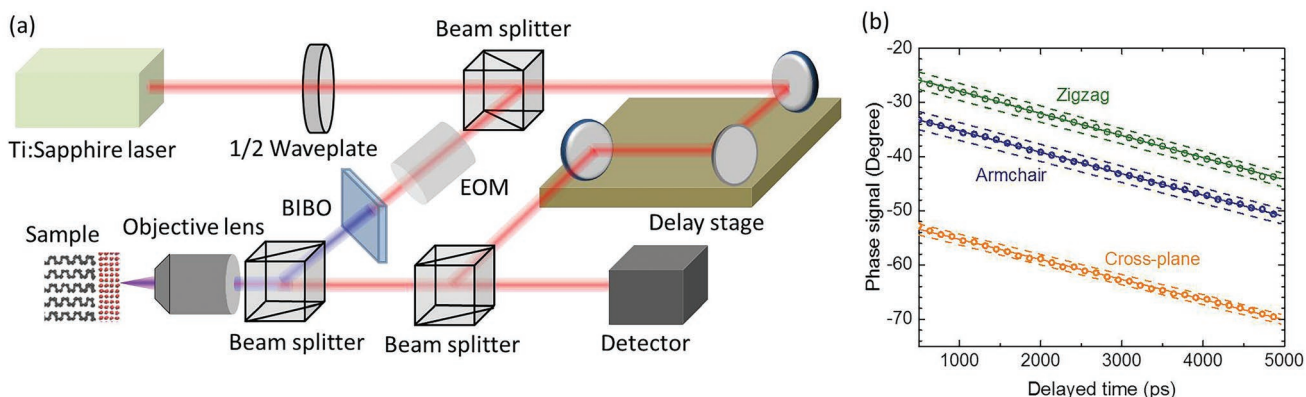


**Figure 2.** Experimental setup of the ultrafast pump–probe spectroscopy and the measurements of anisotropic TBR. a) Schematic of the TDTR method. Blue and red colors represent the pump and probe beams, respectively. b) Experimental data (circles) and the fits from the multilayer thermal transport model (solid lines) for the TDTR phase signal. Calculated curves (dashed lines) using the TBR varied by  $\pm 10\%$  of best values are plotted to illustrate the measurement sensitivity.

construction of the dynamical matrix.<sup>[45]</sup> We applied the density functional theory (DFT) calculations and finite displacement method to obtain the interatomic force constants corresponding to the equilibrium crystal structures.<sup>[45,48,49]</sup> The interlayer van der Waals interaction was corrected by using the DFT-D functionals.<sup>[50]</sup> The lattice constants for the calculated equilibrium structure of Al and BP were compared with the experimental values<sup>[51,52]</sup> and were in good agreement. Under the equilibrium structure, the phonon band structures can be calculated by extracting the second-order force constants by displacing the atoms with a finite distance. More details for the atomistic calculations can be found in the Supporting Information. Note that the TBR here is dominated by phonon transport across the Al–BP interfaces<sup>[53,54]</sup> and we notice that electron–phonon coupling can show importance across some metal–dielectric interfaces.<sup>[55,56]</sup> To verify our calculation results, the calculated phonon dispersion relationships along different directions were compared to experimental data from neutron scattering experiments,<sup>[57,58]</sup> showing good consistency (Figure 3a–d).

TBR is considered as how resistive it is when phonons from both sides participate in thermal transport across the interface. Here, we compare the phonon band structures of BP and Al. Al has three acoustic phonon branches with frequency up to 10 THz. By contrast, BP has three acoustic branches from 0 to ≈6 THz and nine optical branches, three of which are from ≈2 to 8 THz and the other six above 10 THz. Considering energy

conservation during the interface transport and the low probability of scattering events involving multiple phonons, since there is no energy state with comparably high frequency available in Al, the high-frequency phonons inside BP make negligible contributions to the interfacial phonon transport. The highest cutoff frequencies of acoustic phonons along the ZZ, AC, and CP directions will be determined by that of BP, i.e., 5.6, 4.1, and 2 THz, respectively. The CP direction has the largest mismatch of highest cutoff frequencies between the two materials, the AC direction the second, and the ZZ direction the smallest, which qualitatively explains the formation of anisotropic TBRs. In addition, we also noticed that the variations in the phonon traveling velocity distributions along different directions (Figure 3e) can further amplify the anisotropic TBRs: phonon velocity along the ZZ direction has a distribution for higher values than those along the AC and CP directions.

More quantitatively, the TBRs along different directions are carefully calculated in the following. From the detailed balance, at equilibrium and under elastic scattering assumption, the heat flux carried by phonons with a certainty frequency  $\omega_0$  from side A to side B is equal to that from side B to side A<sup>[44]</sup>

$$\begin{aligned} & \sum_i \int_{\mathbf{k}} \tau_{AB}(\mathbf{k}, i) \hbar \omega(\mathbf{k}, i) |\mathbf{v}(\mathbf{k}, i) \cdot \mathbf{n}| f \delta_{\omega_0, \omega(\mathbf{k}, i)} d\mathbf{k} \\ & = \sum_j \int_{\mathbf{k}} \tau_{BA}(\mathbf{k}, j) \hbar \omega(\mathbf{k}, j) |\mathbf{v}(\mathbf{k}, j) \cdot \mathbf{n}| f \delta_{\omega_0, \omega(\mathbf{k}, j)} d\mathbf{k} \end{aligned} \quad (2)$$

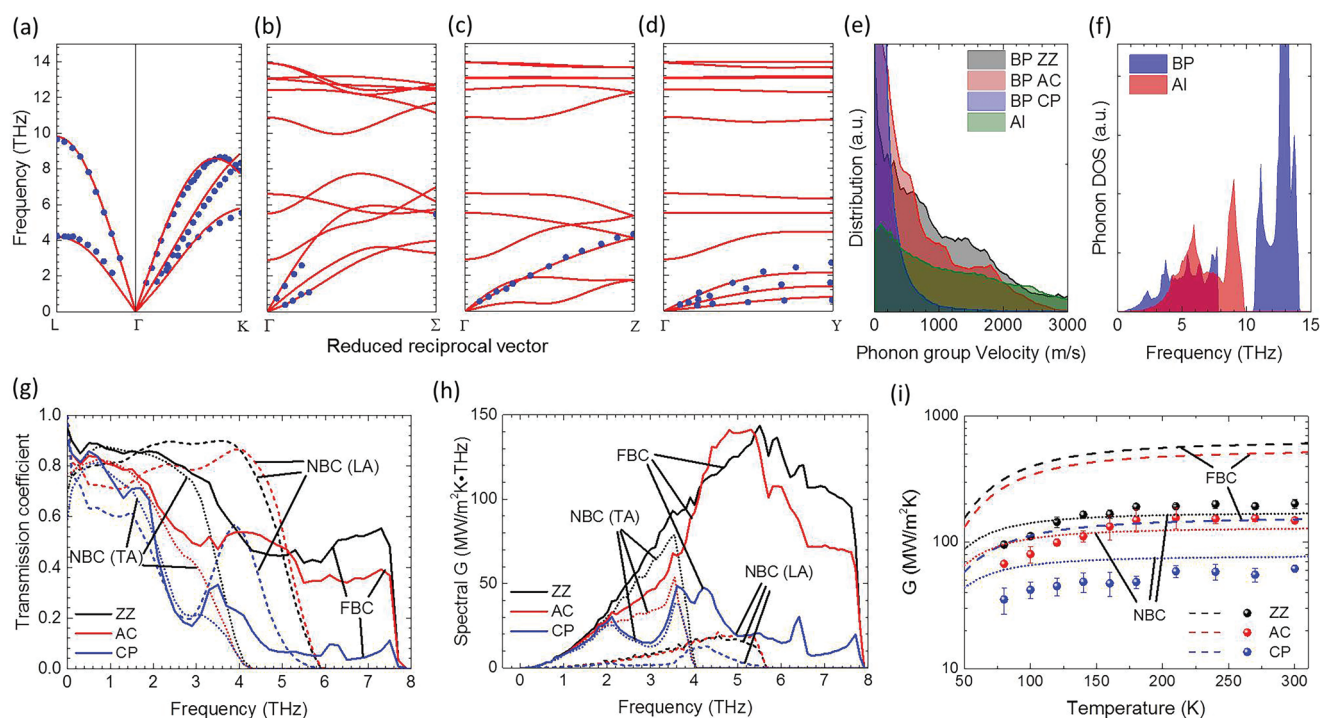


**Figure 3.** Ab initio calculation of phonon band structures and atomistic modeling of phonon spectral contribution to the anisotropic TBRs, in comparison with experimental measurements. a–d) Phonon dispersion relations calculated from DFT (red lines) in comparison with neutron scattering experiments (blue dots<sup>[54,55]</sup>) for Al (a) and BP (b–d). e) Phonon spectral distribution of group velocity in the first Brillouin zone along different crystal directions. f) Phonon spectral distribution of density of states. g) Phonon-mode-dependent transmission coefficients at the Al–BP interface calculated from the FBC and NBC diffuse mismatch models. h) Spectral  $G$  as a function of phonon frequency calculated from FBC and NBC. i) Experimentally measured TBRs (dots) of Al–BP interfaces in comparison to calculations (lines), considering temperature dependence and different crystal orientations.

$$\tau_{AB}(\mathbf{k}, i) = 1 - \tau_{BA}(\mathbf{k}, i) \quad (3)$$

Thus, the transmission coefficient can be calculated as follows:

$$\tau_{AB}(\mathbf{k}, i) = \frac{\sum_i \int_{\mathbf{k}}^{\text{Side B}} |\mathbf{v}(\mathbf{k}, j) \mathbf{n}| \delta_{\omega_0, \omega(\mathbf{k}, j)} d\mathbf{k}}{\sum_i \int_{\mathbf{k}}^{\text{Side A}} |\mathbf{v}(\mathbf{k}, i) \mathbf{n}| \delta_{\omega_0, \omega(\mathbf{k}, i)} d\mathbf{k} + \sum_j \int_{\mathbf{k}}^{\text{Side B}} |\mathbf{v}(\mathbf{k}, j) \mathbf{n}| \delta_{\omega_0, \omega(\mathbf{k}, j)} d\mathbf{k}} \quad (4)$$

where  $\delta_{\omega_0, \omega(\mathbf{k}, i)}$  is the Kronecker delta function.  $\tau_{AB}(\mathbf{k}, i)$  is a key parameter to quantify TBR, but remains challenging for state-of-the-art phonon theories. Note that one implicit assumption in most literature modeling is that all the phonons lose their memory of their polarization after being diffusely scattered at the interface. However, phonons may not be able to hop across different branches freely. The determination of the probability of the phonons to jump between different branches is non-trivial. Although some recent work based on atomic Green's function investigated the modeling of the phonon mode conversion,<sup>[59,60]</sup> these studies are limited to ideal interfaces with atomic-level perfection. Therefore, we performed calculations for both extreme cases, i.e., free branch conversion (FBC) and no branch conversion (NBC) based on diffuse mismatch model (DMM). In FBC-DMM, the phonon flux balance is calculated without being specified to a certain polarization. In NBC-DMM, the transmission coefficient was calculated for longitudinal acoustic (LA) branches and transversely acoustic (TA) branches separately by using Equation (4).

To analyze the phonon spectral transport at the interface, the phonon spectral interface transmission coefficients ( $\tau_{AB}$ ) for different orientations were calculated based on FBC-DMM and NBC-DMM and shown in Figure 3g. The FBC-DMM transmission coefficients show a frequency with a nearly monotonically decreasing trend followed by a sharp drop to zero at 7.9 THz. The sudden drop of transmissivities can be explained by the phonon density of states (PDOS) of Al and BP (Figure 3f). The phonons with frequencies from 7.9 to 9.8 THz allowed on the Al side are not allowed on the BP side, leading to no open channels for these phonons at the interface. Figure 3f also shows that, for example, the PDOS ratio of BP and Al is higher than 1 before around 4 THz, and decreases from  $\approx 4$  to  $\approx 6$  THz, thus resulting in a similar trend for the transmission coefficients. In addition, the reduced phonon group velocity near the Brillouin zone edge is also responsible for the decreasing transmission coefficients. In the NBC-DMM, the transmission coefficients can be decomposed into contributions from LA and TA phonons. The transmission coefficients become zero when frequencies of LA phonons and TA phonons reach their highest values.

The TBRs are calculated based on both FBC-DMM and NBC-DMM. These two models lead to different interface spectral transmissivities (Figure 3g) and thus different phonon spectral contribution to TBR. The spectral interface thermal conductance  $G$  (i.e.,  $1/\text{TBR}$ ) for the Al–BP interface is decomposed into relative contributions from different phonon modes and displayed in Figure 3h. For almost the full frequency range,  $G$  along the cross-plane direction is lowest regardless of the model used, because of the smallest phonon energy and group velocity in the cross-plane direction. Despite the different

absolute magnitudes, the most significant difference in spectral  $G$  between these two models lies in the contribution from high-energy phonons (e.g., frequency  $>4$  THz, which is the cutoff frequency of TA phonons in BP). According to the FBC-DMM prediction, the optical phonons with frequencies between 2.1 and 7.8 THz dominate the interfacial thermal transport, whereas the NBC-DMM ignores the contribution from optical phonons. In the FBC-DMM, peaks are around 4–6 THz, where both the optical phonons and LA phonons exist with relatively high group velocity. The maximum frequency of phonons contributing to  $G$  in the NBC-DMM is around 5.6 THz, up to which phonons are allowed on three acoustic bands.

Furthermore, this distinct phonon spectral contribution to interface thermal transport can be observed from its temperature dependence because the excitation of higher energy phonons is more temperature dependent. We calculated temperature-dependent  $G$  from 50 to 300 K using both FBC-DMM and NBC-DMM in Figure 3i. We have also plotted our experimentally measured temperature-dependent  $G$  in the same figure for comparison. First, it is clear that the NBC-DMM prediction has a better agreement with the experimental measurement in terms of the magnitude of TBR. On the other hand, it is interesting to notice that the FBC-DMM predicts a stronger temperature effect (i.e., a higher slope of temperature-dependent  $G$ ) than NBC-DMM, indicating that optical phonons partially participate in the interfacial thermal transport. To involve the optical phonon transport at interface, it requires the mode conversion from acoustic phonons in Al to optical phonons in BP. The probability for phonon mode conversion across different branches is important for phonon theory but difficult to be determined. Recently, atomic Green's function (AGF) was combined with DFT calculations to treat the mode conversion,<sup>[59,60]</sup> but it is challenging to include anharmonic effects into AGF. Molecular dynamics simulation, on the other hand, can be an alternative tool to study interfacial thermal transport by implicitly considering the phonon mode conversion and full-order anharmonic effects.<sup>[19,61]</sup>

To further quantify TBR between Al and BP along the different crystal directions and phonon mode conversion across branches, we performed the nonequilibrium molecular dynamics (MD) simulations. In the MD simulation domain illustrated in Figure 4a, BP is sandwiched by two Al blocks. A periodic boundary condition is applied to all the directions and the real structure can be interpreted as an Al/BP superlattice, with heat source and heat sink layers lying in the center of BP and Al. Application of heat current through the heat source to the heat sink forms a temperature gradient along the direction normal to the interface. By monitoring the temperature drop ( $\Delta T$ ) across the interface, the thermal boundary conductance can be calculated from  $G = Q/\Delta T$ . In our simulation, the embedded-atom method empirical potential<sup>[62]</sup> was used for describing the interaction between Al atoms. The Stillinger–Weber potential and Lennard–Jones (LJ) potential were adopted for the intra- and interplane interactions in BP, respectively.<sup>[62–64]</sup> The interfacial interaction between Al and BP was simulated using LJ potential  $V_{ij} = 4\epsilon[(\sigma/r_{ij})^{12} - (\sigma/r_{ij})^6]$ , where  $\epsilon$  is the interatomic energy and  $\sigma$  is the distance corresponding to the zero potential energy.<sup>[64,65]</sup> More details for the MD simulations can be found in the Supporting Information.

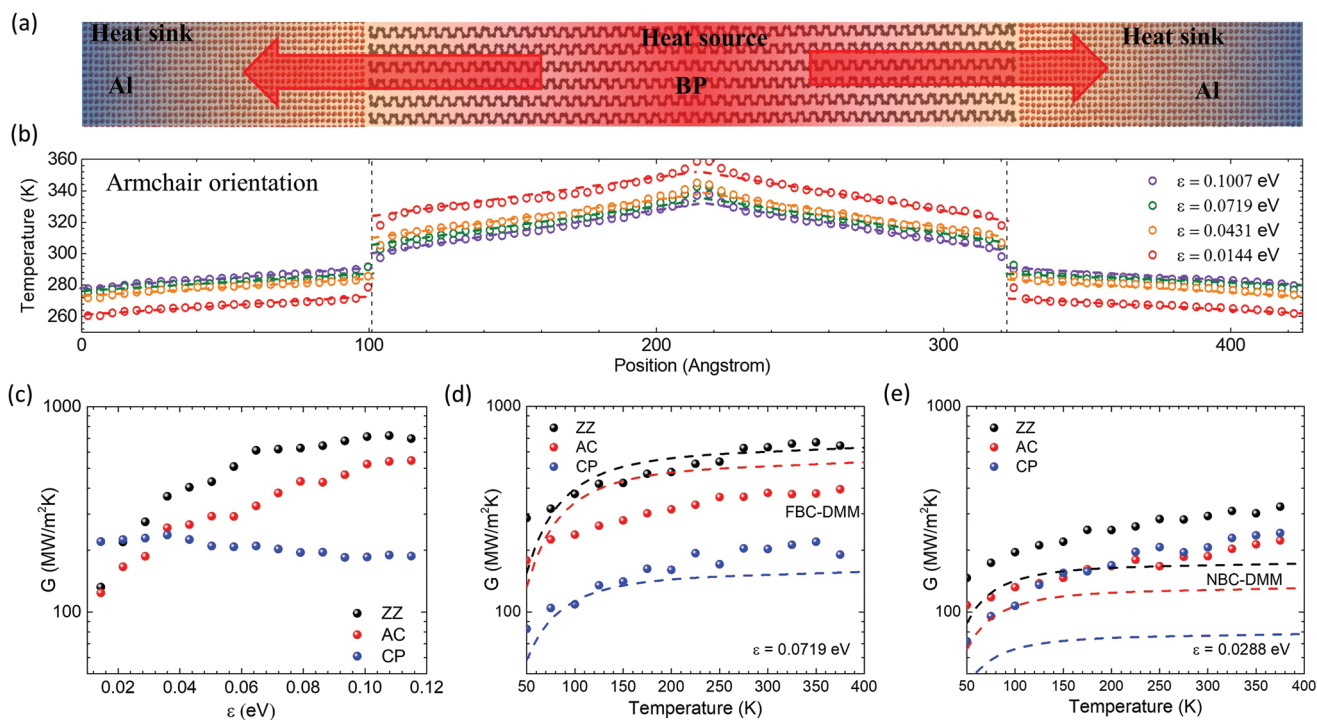


**Figure 4.** MD simulation of anisotropic TBRs. a) Schematic of MD simulations for interfaces with different orientations. b) Steady-state temperature profiles across the interfaces calculated using different interatomic energies ( $\epsilon$ ) under a constant heat flux. c) Calculated anisotropic TBRs as a function of  $\epsilon$  at 300 K. d, e) TBRs in comparison between MD simulations (dots) and DMM calculations for  $\epsilon = 0.0719$  and  $0.0288$  eV, respectively, considering three characteristic crystal orientations.

The steady-state temperature profiles of the BP–Al system for different crystal directions are predicted by the MD simulation and shown in Figure 4b. Here, a key parameter, the interatomic energy  $\epsilon$ , is varied to study the effects from the interfacial bonding between BP and Al on the TBR. It is interesting to notice that the anisotropic TBR has a strong dependence on  $\epsilon$ , and there is a transition point around 0.03 eV (Figure 4c). A larger  $\epsilon$  stands for a stronger bonding between atoms across the interface and reduces TBR, and also potentially affects phonon conversion between different branches. When  $\epsilon > 0.03$  eV, MD simulation predicts  $TBR_{ZZ} < TBR_{AC} < TBR_{CP}$ , which is consistent with the experimental results and DMM calculations. Note that the value of  $\epsilon$  for BP–Al interface can be estimated following the Lorentz–Berthelot rules,<sup>[66]</sup> to be around  $\epsilon_0 = 0.0719$  eV. Interestingly, at  $\epsilon_0$ , the predicted TBRs for the interface with the ZZ and *c* orientations are almost similar to the values calculated with the FBC model (Figure 4d) but deviate from the NBC model (Figure 4e). From the consistency between the MD simulation and FBC model calculations, it can be inferred that phonon mode conversion is relatively strong at the interface along the ZZ and CP directions, but weak (although non-negligible) in the AC direction. Such an observation can be partially attributed to the cross of phonon dispersions of different branches along the ZZ direction as illustrated in Figure 3b, which opens the conversion channel between different branches. At a much lower  $\epsilon$ , for example, 0.03 eV in Figure 4e, the MD simulated TBRs decrease and approach the NBC prediction. Therefore, this study indicates that the strength of interfacial bonding positively correlates with the phonon mode conversion at interface.

In summary, we report for the first time a systematic characterization of anisotropic interfacial phonon transport across metal–semiconductor material interfaces. A record-high anisotropic ratio of TBR of 3.27 has been experimentally measured due to the strongly anisotropic phonon band structures of black phosphorus. The spectral transmissivity of phonon transport across interfaces with different orientations has been analyzed by using ab initio calculated full phonon dispersions from DFT. The temperature-dependent anisotropic TBR measurement and DMM calculations suggest the existence of phonon conversion between different branches under phonon gas theory. Moreover, molecular dynamics simulation was performed to implicitly include all the anharmonic effects and phonon mode conversion and shows consistency with experimental results. Our experimental measurements and theoretical calculations of the thermal transport at the metal–semiconductor interface provide a detailed fundamental understanding of TBR–structure relationships. This knowledge provides important guidance for improving the thermal boundary resistance in nanoscale electronic devices, and may open up new opportunities in the rational design and control of novel interface materials for advanced thermal management technologies. Note that BP serves as a proof-of-concept study in this work, but such anisotropic interface energy transport can be extended to more energy forms and wide range of systems such as layered materials, superlattices, and any inhomogeneous structures. We also expect that such anisotropic TBRs are becoming more important for scale-down device structures in 3D and at the nanoscale. In addition, how to take the

advantage of interface anisotropy to design new device operation schemes, for example, thermal switch or thermal diode for thermal management, could be other interesting research directions.

## Supporting Information

Supporting Information is available from the Wiley Online Library or from the author.

## Acknowledgements

Y.H. acknowledges the support from an Alfred P. Sloan Research Fellowship, a CAREER award from the National Science Foundation, a Young Investigator Award from the US Air Force Office of Scientific Research, and a Doctoral New Investigator Award from the American Chemical Society Petroleum Research Fund, as well as from the UCLA Sustainable LA Grand Challenge and the Anthony and Jeanne Pritzker Family Foundation. The authors thank H. Albrecht for the helpful discussion. This work used the Extreme Science and Engineering Discovery Environment (XSEDE), which was supported by National Science Foundation grant no. ACI-1548562.

Note: When initially published, the caption of Figure 4d,e misleadingly indicated that these parts of Figure 4 contain experimental data. The caption was updated on August 13, 2019 to correct this, after initial publication online.

## Conflict of Interest

The authors declare no conflict of interest.

## Keywords

2D materials, interface phonon transmission, thermal management, time-domain thermoreflectance (TDTR) measurements

Received: February 12, 2019

Revised: May 19, 2019

Published online: June 24, 2019

- [1] P. Ball, *Nature* **2012**, 492, 174.
- [2] M. M. Waldrop, *Nature* **2016**, 530, 144.
- [3] A. Bar-Cohen, P. Wang, in *Nano-Bio-Electronic, Photonic and MEMS Packaging* (Eds: C. P. Wong, K.-S. Moon, Y. Li), Springer, New York **2010**, pp. 349–429.
- [4] A. Sood, E. Pop, M. Asheghi, K. E. Goodson, in *17th IEEE Inter-society Conf. on Thermal and Thermomechanical Phenomena in Electronic Systems*, IEEE, Piscataway, NJ, USA **2018**, pp. 1396–1402.
- [5] *International Technology Roadmap for Semiconductors (ITRS)*, 2015 ed., Semiconductor Industry Association, Washington, DC, USA **2015**, <http://www.itrs2.net/> (accessed: January 2019).
- [6] A. Shehabi, S. Smith, D. Sartor, R. Brown, M. Herrlin, J. Koomey, E. Masanet, N. Horner, I. Azevedo, W. Lintner, *United States Data Center Energy Usage Report*, Berkeley National Laboratory, Berkeley, CA, USA **2016**.
- [7] J. S. Kang, M. Li, H. Wu, H. Nguyen, Y. Hu, *Science* **2018**, 361, 575.
- [8] J. S. Kang, H. Wu, Y. Hu, *Nano Lett.* **2017**, 17, 7507.
- [9] Y. Hu, L. Zeng, A. J. Minnich, M. S. Dresselhaus, G. Chen, *Nat. Nanotechnol.* **2015**, 10, 701.
- [10] E. Pop, S. Sinha, K. E. Goodson, *Proc. IEEE* **2006**, 94, 1587.
- [11] A. A. Balandin, *Nat. Mater.* **2011**, 10, 569.
- [12] Y. Won, J. Cho, D. Agonafer, M. Asheghi, K. E. Goodson, *IEEE Trans. Compon., Packag., Manuf. Technol.* **2015**, 5, 737.
- [13] S. Li, S. Li, Q. Zheng, Y. Lv, X. Liu, X. Wang, P. Y. Huang, G. David, B. Lv, *Science* **2018**, 361, 579.
- [14] F. Tian, B. Song, X. Chen, N. K. Ravichandran, Y. Lv, K. Chen, S. Sullivan, J. Kim, Y. Zhou, T. H. Liu, M. Goni, Z. Ding, J. Sun, G. A. G. U. Gamage, H. Sun, H. Ziyae, S. Huyan, L. Deng, J. Zhou, A. J. Schmidt, S. Chen, C. W. Chu, P. Y. Huang, D. Broido, L. Shi, G. Chen, Z. Ren, *Science* **2018**, 361, 582.
- [15] A. Bar-Cohen, J. D. Albrecht, J. J. Maurer, in *Technical Digest—IEEE Compound Semiconductor Integrated Circuit Symp. (CSIC)*, IEEE, Piscataway, NJ, USA **2011**, pp. 1–5.
- [16] N. P. Padture, M. Gell, E. H. Jordan, *Science* **2002**, 296, 280.
- [17] G. L. Pollack, *Rev. Mod. Phys.* **1969**, 41, 48.
- [18] E. T. Swartz, R. O. Pohl, *Rev. Mod. Phys.* **1989**, 61, 605.
- [19] C. Monachon, L. Weber, C. Dames, *Annu. Rev. Mater. Res.* **2016**, 46, 433.
- [20] K. S. Novoselov, D. Jiang, F. Schedin, T. J. Booth, V. V. Khotkevich, S. V. Morozov, A. K. Geim, *Proc. Natl. Acad. Sci. USA* **2005**, 102, 10451.
- [21] Q. H. Wang, K. Kalantar-Zadeh, A. Kis, J. N. Coleman, M. S. Strano, *Nat. Nanotechnol.* **2012**, 7, 699.
- [22] W. Xu, W. Liu, J. F. Schmidt, W. Zhao, X. Lu, T. Raab, C. Diederichs, W. Gao, D. V. Seletskiy, Q. Xiong, *Nature* **2017**, 541, 62.
- [23] P. Rivera, K. L. Seyler, H. Yu, J. R. Schaibley, J. Yan, D. G. Mandrus, W. Yao, X. Xu, *Science* **2016**, 351, 688.
- [24] Z. Lin, Y. Liu, U. Halim, M. Ding, Y. Liu, Y. Wang, C. Jia, P. Chen, X. Duan, C. Wang, *Nature* **2018**, 562, 254.
- [25] X. Ling, H. Wang, S. Huang, F. Xia, M. S. Dresselhaus, *Proc. Natl. Acad. Sci. USA* **2015**, 112, 4523.
- [26] A. Morita, *Appl. Phys. A: Solids Surf.* **1986**, 39, 227.
- [27] P. W. Bridgman, *J. Am. Chem. Soc.* **1914**, 36, 1344.
- [28] J. S. Kang, M. Ke, Y. Hu, *Nano Lett.* **2017**, 17, 1431.
- [29] H. Jang, J. D. Wood, C. R. Ryder, M. C. Hersam, D. G. Cahill, *Adv. Mater.* **2015**, 27, 8017.
- [30] Z. Luo, J. Maassen, Y. Deng, Y. Du, R. P. Garrelts, M. S. Lundstrom, P. D. Ye, X. Xu, *Nat. Commun.* **2015**, 6, 8572.
- [31] B. Smith, B. Vermeersch, J. Carrete, E. Ou, J. Kim, N. Mingo, D. Akinwande, L. Shi, *Adv. Mater.* **2017**, 29, 1603756.
- [32] S. Lee, F. Yang, J. Suh, S. Yang, Y. Lee, G. Li, H. S. Choe, A. Suslu, Y. Chen, C. Ko, J. Park, K. Liu, J. Li, K. Hippalgaonkar, J. J. Urban, S. Tongay, J. Wu, *Nat. Commun.* **2015**, 6, 8573.
- [33] B. Sun, X. Gu, Q. Zeng, X. Huang, Y. Yan, Z. Liu, R. Yang, Y. K. Koh, *Adv. Mater.* **2017**, 29, 1603297.
- [34] J. Zhu, H. Park, J. Y. Chen, X. Gu, H. Zhang, S. Karthikeyan, N. Wendel, S. A. Campbell, M. Dawber, X. Du, M. Li, J. P. Wang, R. Yang, X. Wang, *Adv. Electron. Mater.* **2016**, 2, 1600040.
- [35] S. Sugai, I. Shirovani, *Solid State Commun.* **1985**, 53, 753.
- [36] J. Wu, N. Mao, L. Xie, H. Xu, J. Zhang, *Angew. Chem.* **2015**, 127, 2396.
- [37] A. L. Phaneuf-L'Heureux, A. Favron, J. F. Germain, P. Lavoie, P. Desjardins, R. Leonelli, R. Martel, S. Francoeur, *Nano Lett.* **2016**, 16, 7761.
- [38] M. Li, J. S. Kang, Y. Hu, *Rev. Sci. Instrum.* **2018**, 89, 084901.
- [39] A. J. Schmidt, X. Chen, G. Chen, *Rev. Sci. Instrum.* **2008**, 79, 114902.
- [40] D. G. Cahill, *Rev. Sci. Instrum.* **2004**, 75, 5119.
- [41] D. G. Cahill, P. V. Braun, G. Chen, D. R. Clarke, S. Fan, K. E. Goodson, P. Keblinski, W. P. King, G. D. Mahan, A. Majumdar, H. J. Maris, S. R. Phillpot, E. Pop, L. Shi, *Appl. Phys. Rev.* **2014**, 1, 011305.
- [42] A. J. Schmidt, K. C. Collins, A. J. Minnich, G. Chen, *J. Appl. Phys.* **2010**, 107, 104907.

- [43] L. Zeng, K. C. Collins, Y. Hu, M. N. Luckyanova, A. A. Maznev, S. Huberman, V. Chiloyan, J. Zhou, X. Huang, K. A. Nelson, *Sci. Rep.* **2015**, *5*, 17131.
- [44] G. Chen, *Nanoscale Energy Transport and Conversion: A Parallel Treatment of Electrons, Molecules, Phonons, and Photons*, Oxford University Press, New York **2005**.
- [45] M. T. Dove, M. T. Dove, *Introduction to Lattice Dynamics*, Cambridge University Press, Cambridge, UK **1993**.
- [46] P. Reddy, K. Castelino, A. Majumdar, *Appl. Phys. Lett.* **2005**, *87*, 211908.
- [47] Z. Chen, Z. Wei, Y. Chen, C. Dames, *Phys. Rev. B* **2013**, *87*, 125426.
- [48] S. Baroni, S. de Gironcoli, A. Dal Corso, P. Giannozzi, *Rev. Mod. Phys.* **2001**, *73*, 515.
- [49] A. Togo, I. Tanaka, *Scr. Mater.* **2015**, *108*, 1.
- [50] S. Grimme, *J. Comput. Chem.* **2006**, *27*, 1787.
- [51] A. Brown, S. Rundqvist, *Acta Crystallogr.* **1965**, *19*, 684.
- [52] W. P. Davey, *Phys. Rev.* **1925**, *25*, 753.
- [53] A. Majumdar, P. Reddy, *Appl. Phys. Lett.* **2004**, *84*, 4768.
- [54] H. C. Chien, D. J. Yao, C. T. Hsu, *Appl. Phys. Lett.* **2008**, *93*, 231910.
- [55] L. Guo, S. L. Hodson, T. S. Fisher, X. Xu, *J. Heat Transfer* **2012**, *134*, 042402.
- [56] Z. Lu, Y. Wang, X. Ruan, *Phys. Rev. B* **2016**, *93*, 064302.
- [57] R. Stedman, G. Nilsson, *Phys. Rev.* **1966**, *145*, 492.
- [58] Y. Fujii, Y. Akahama, S. Endo, S. Narita, Y. Yamada, G. Shirane, *Solid State Commun.* **1982**, *44*, 579.
- [59] S. Sadasivam, U. V. Waghmare, T. S. Fisher, *Phys. Rev. B* **2017**, *96*, 174302.
- [60] Z. Y. Ong, G. Zhang, *Phys. Rev. B* **2015**, *91*, 174302.
- [61] Y. Zhou, M. Hu, *Phys. Rev. B* **2017**, *95*, 115313.
- [62] K. W. Jacobsen, J. K. Nørskov, M. J. Puska, *Phys. Rev. B* **1987**, *35*, 7423.
- [63] J.-W. Jiang, *Nanotechnology* **2015**, *26*, 315706.
- [64] Y.-Y. Zhang, Q.-X. Pei, J.-W. Jiang, N. Wei, Y.-W. Zhang, *Nanoscale* **2016**, *8*, 483.
- [65] P. Puri, V. Yang, *J. Phys. Chem. C* **2007**, *111*, 11776.
- [66] T. Luo, J. R. Lloyd, *Adv. Funct. Mater.* **2012**, *22*, 2495.